

## Achieving room-temperature superplasticity in an ultrafine-grained Zn-22% Al alloy

T. Uesugi<sup>1</sup>, Y. Takigawa<sup>1</sup>, M. Kawasaki<sup>1,2</sup>, K. Higashi<sup>1†</sup>

†higashi@mtr.osakafu-u.ac.jp

<sup>1</sup>Department of Materials Science, Osaka Prefecture University, 1—1 Gakuen-sho, Naka-ku, Sakai, Osaka 599—8531, Japan

<sup>2</sup>Division of Materials Science and Engineering, Hanyang University, 222 Wangsimni-ro, Seongdong-gu, Seoul 133—791, South Korea

The mechanisms of creep and superplasticity occurring in conventional coarse-grained materials are now understood well. However, recent study advances in the production of bulk metals with submicrometer grain sizes which provide the opportunity to demonstrate improved mechanical properties. Thermo-mechanical processing is used in conventional industrial practice to achieve substantial grain refinement in bulk metals whereas the smallest grain sizes achieved in this way are of the order of a few micrometers and generally it is not possible to achieve grain sizes within the submicrometer or nanometer range. In this report, synthesis of an ultrafine-grained Zn-22% Al eutectoid alloy was demonstrated through solutionizing followed by thermo-mechanical processing. Microstructural investigations revealed there are stable equiaxed ultrafine grain sizes of  $\sim 0.63 \mu\text{m}$  with homogeneous distributions of Zn and Al grains. Tensile testing demonstrated the occurrence of excellent room-temperature superplasticity with a maximum elongation of 400% at a strain rate of  $1.0 \times 10^{-3} \text{ s}^{-1}$  where the elongation is one of the highest room-temperature superplastic elongation recorded to date in Zn-22% Al alloy. However, the strain rate sensitivity of superplastic flow was measured as  $\sim 0.24$  which is lower than the theoretical value of  $\sim 0.5$  for conventional superplasticity. The present study estimates a threshold stress as one of possible reasons for lowering the strain rate sensitivity of room-temperature superplastic flow in the ultrafine-grained Zn-22% Al alloy.

**Keywords:** elongation, strain rate sensitivity, superplasticity, ultrafine grained microstructure, Zn-Al alloy

## Достижение сверхпластичности ультрамелкозернистого сплава Zn-22% Al при комнатной температуре

Механизмы процессов ползучести и сверхпластичности, имеющих место в крупнозернистых материалах, в настоящее время хорошо поняты. Однако недавние исследования привели к успехам в получении объемных образцов металлов с субмикронным размером зерен, которые предоставляют возможность демонстрации улучшенных механических свойств. В традиционной промышленной практике для достижения существенного измельчения зерен используется термомеханическая обработка, но наименьшие размеры зерен, достигаемые этим способом, составляют величину порядка нескольких микрометров, и с их помощью обычно невозможно достигать размеров зерен в субмикрометрическом или нанометровом диапазоне. В настоящей работе продемонстрировано получение ультрамелкозернистого эвтектидного сплава Zn-22% Al путем обработки на твердый раствор с последующей термомеханической обработкой. Микроструктурные исследования показали, что в результате такой обработки образуются стабильные равноосные ультрамелкие зерна размерами около  $0.63 \mu\text{m}$  с однородным распределением зерен Zn и Al. Испытания растяжением показали проявление превосходной сверхпластичности при комнатной температуре с максимальным удлинением 400% при скорости деформации  $1.0 \times 10^{-3} \text{ c}^{-1}$ . Полученное удлинение является одним из наиболее высоких сверхпластических удлинений при комнатной температуре, зарегистрированных до настоящего времени на сплаве Zn-22% Al. Однако измеренное значение скоростной чувствительности сверхпластического течения, равное примерно 0.24, ниже, чем теоретическое значение для традиционной сверхпластичности, равное 0.5. В настоящей работе оценено пороговое напряжение, которое является одной из возможных причин уменьшения скоростной чувствительности сверхпластичности при комнатной температуре в ультрамелкозернистом сплаве Zn-22%.

**Ключевые слова:** удлинение, параметр скоростной чувствительности, сверхпластичность, ультрамелкозернистая структура, сплав Zn-Al

## 1. Introduction

Superplastic ductility refers to exceptionally high elongation of at least 400% [1] without necking when testing in tension at elevated temperature of  $T \geq 0.5T_m$  ( $T_m$ : the absolute melting temperature). In conventional superplastic metals, it is well known that the flow within the superplastic regime occurs by grain boundary sliding (GBS) [2] and the extensive cavitation develops internally when materials pull out to significant superplastic elongations [3]. It is worth recalling in the special issue on superplasticity that there are three major papers published in the last three decades that still record the maximum superplastic elongations in conventional metallic materials [4–6].

A Zn-22% Al eutectoid alloy is recognized as a highly superplastic material in conventional testing [7–9]. Research over the last two decades has had a special focus on the microstructural refinement of materials and established the potential for attaining smaller grain sizes, typically in the submicrometer range, which lead to superior mechanical properties [10]. There have been numerous trials of grain refinement for improving superplastic properties of Zn-22% Al alloys by means of the techniques of cross-channel extrusion (CCE) [11], equal-channel angular pressing (ECAP) [12], friction stir processing (FSP) [13], high-pressure torsion (HPT) [14] and thermo-mechanical controlling process (TMCP) [15]. These processing techniques led to refine grains of Zn-22% Al alloys to the submicrometer range so that the alloys exhibited superplastic characteristics including excellent ductility at elevated temperature [16–21] and superplastic flow behavior even at room temperature [22–31]. Recent reports examined the capability of room-temperature superplastic properties in Zn-22% Al alloys as tuned mass dampers to reduce seismic vibrations in building structures [32,33].

In earlier references, however, several different Zn-Al alloys with mostly small amount of Al content were produced through conventional thermo-mechanical processing, such as cold/hot-rolling, to have ultrafine-grained microstructures [34–39]. Accordingly, the present study was initiated to demonstrate the feasibility of producing an ultrafine-grained Zn-22% Al alloy with using conventional thermo-mechanical processing without utilizing any special grain refinement technique. The produced alloy was examined in tension for evaluating superplastic properties at room temperature. The results are compared with published experimental reports demonstrating superplastic and superplastic-like properties at room temperature in a range of Zn-Al alloys. Moreover, special emphasis was placed to discuss the possible reasons of lowering the strain rate sensitivity of the observed true superplastic flow in an ultrafine-grained Zn-22% Al alloy.

## 2. Experimental materials and synthesis of an ultrafine-grained Zn-22% Al alloy

A Zn-22% Al eutectoid alloy was prepared by casting an Al (99.999%) and a Zn (99.99%) in an Ar atmosphere. In specific, the Zn-Al alloy contains 22.0 wt.% of Al with 110

wt.ppm Si as a major impurity. The manufacturing processes were operated with care so that each impurity contents of Fe, Cu, Pb, Mg and Cd was controlled to fall under 10 ppm.

After casting, solution treatments were conducted precisely to introduce uniformly distributed equiaxed Al-rich and Zn-rich grains in a binary microstructure. In specific, the as-cast alloy was heated slowly to achieve 633 K in 9 hours and solutionized at the consistent temperature for 15 hours followed by quenching using iced water. It should be mentioned that the solutionization process is very critical for removing an initial non-homogeneous microstructure introduced during casting and the optimal conditions of solutionizing as described above were selected after several experimental trials. Figure 1 demonstrates representative SEM photos showing (a) an incomplete microstructure of solutionizing (reaching 633 K in 4 hours and holding time of 8 hours) and (b) a complete microstructure of solutionizing (reaching 633 K in 9 hours and holding time of 15 hours) in the Zn-22% Al alloy. It should be noted that the grains appearing white are the Zn grains and the dark grains are Al. It is apparent that the optimal solutionizing condition gives fully homogeneous two-phase microstructure as shown in Fig. 1b whereas the incompletely solutionized microstructure shows non-uniform distributions of Al and Zn phases consisting of equiaxed grains and lamellae as shown in Fig. 1a.

The alloy is then cold rolled into a plate having a thickness of ~2 mm and a set of tensile specimens was machined from the plate to have a gauge length of 10 mm and a cross-section area of 6.0×1.5 mm<sup>2</sup> where the gauge lengths were oriented parallel to the rolling direction. In order to stabilize the microstructure in the specimens after cold rolling, the

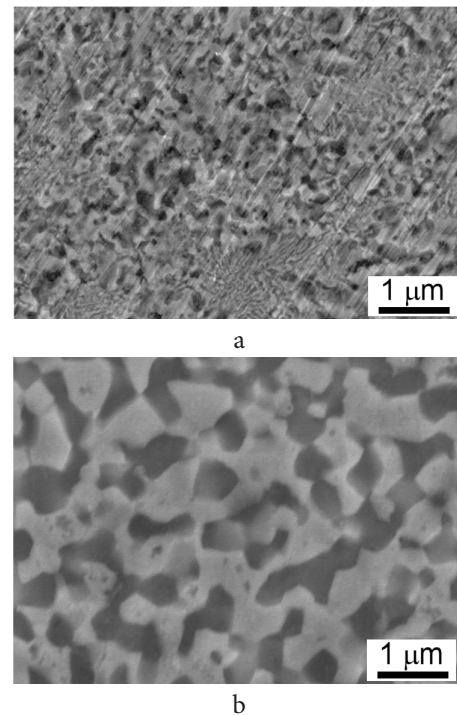


**Fig. 1.** Representative SEM photos showing (a) an incomplete microstructure of solutionizing (reaching 633 K in 4 hours and holding time of 8 hours) and (b) a complete microstructure of solutionizing (reaching 633 K in 9 hours and holding time of 15 hours) in the Zn-22% Al alloy.

samples were annealed at 423 K for 1 hour prior to testing.

The initial microstructure was examined within the gauge perpendicular to the rolling direction of each alloy before tensile testing using an electron backscatter diffraction (EBSD) technique and an orientation imaging microscopy (OIM). The EBSD analysis was undertaken using a JEOL JSM 7001F scanning electron microscope (SEM) and the EBSD patterns were collected with TSL OIM software at the observed areas of  $20 \times 7 \mu\text{m}^2$  with taking a step size of  $0.05 \mu\text{m}$  and a cut-off angle of  $2^\circ$  for the minimum boundary misorientation. The clean-up procedure was performed in an OIM-TSL analyzer and all scanned datum points having confidence index values of  $\sim 0.01$  were excluded from the data sets to improve the overall precision of the OIM images.

### 3. Experimental results

Figure 2a shows the OIM micrographs of the Zn-22% Al alloy including, from left, all grains, only Zn-rich grains and only Al-rich grains where a set of grain colors for Zn having an h.c.p. crystal structure and for Al having a f.c.c. crystal structure correspond to the orientations in the color unit

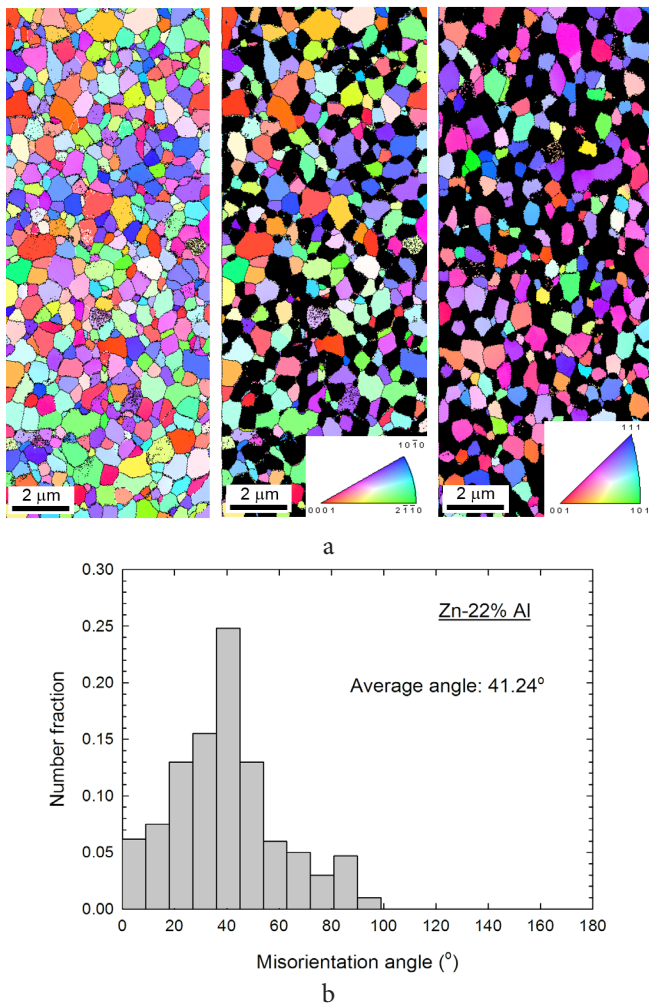


**Fig. 2.** (a) The OIM micrographs of the Zn-Al alloy for, from left, all grains, only Zn-rich grains and only Al-rich grains and (b) the fractions of grain boundaries plotted as a function of the boundary misorientation angle.

triangles at the bottom of each micrographs, respectively. The fractions of grain boundaries plotted as a function of the boundary misorientation angle are shown in Fig. 2b for the Zn-22% Al alloy prior to tensile testing.

It is apparent from Fig. 2a that the high-purity alloy consists of fairly equiaxed fine grains separated by a high fraction of high-angle grain boundaries before testing. The OIM images for the specific phases of Zn and Al show that the alloy includes homogeneously distributed Zn and Al grains in the binary microstructure. Detail investigation revealed the average grain sizes of  $\sim 0.63 \mu\text{m}$  for all grains,  $\sim 0.66 \mu\text{m}$  and  $\sim 0.59 \mu\text{m}$  for the individual Zn and Al grains, respectively, and the average misorientation angle of grain boundaries of  $\sim 41.24^\circ$ . It is worthwhile to note that the fabricated microstructure of the Zn-22% Al alloy after cold rolling followed by annealing is reasonably stable even additional one hour of annealing at 423 K where limited grain growth within  $+0.1 \mu\text{m}$  was shown in both Zn and Al grains.

Tensile testing was conducted at room temperature of 298 K at strain rates of  $10^{-4}$ – $10^{-2} \text{ s}^{-1}$  and a plot of true stress-true strain curves are shown in Fig. 3 and the tensile testing results are summarized in Fig. 4 as plots of elongations to failure (upper) and flow stress (lower) versus strain rate for the Zn-22% Al alloy.

The stress-strain curves in Fig. 3 show that there is a strain rate dependency of yield strength where the flow stress is higher at faster strain rate during testing. It is also apparent that the Zn-Al alloy demonstrates reasonably stable plateau stresses so that excellent ductility is achieved during deformation at room temperature.

The alloy exhibited elongations of  $>200\%$  at all strain rates as shown in an upper plot of Fig. 4 and a maximum elongation of 400% was observed at  $10^{-3} \text{ s}^{-1}$  in the present experiments. The result suggests the ultrafine-grained Zn-22% Al alloy demonstrates true room-temperature superplasticity and the significant superplastic elongation is the highest recorded in Zn-22% Al alloy at room temperature to date. From the lower curve in Fig. 4, the strain rate sensitivity,  $m$ , of  $\sim 0.24$  was calculated under the experimental conditions. Although this value is lower than  $m \approx 0.5$  measured in the alloy showing excellent superplasticity at 473 K [8], it is in good agreement with the earlier reports demonstrating  $m \approx 0.2$ – $0.4$  for superplastic-type characteristics in Zn-22% Al alloys when testing in tension at room temperature

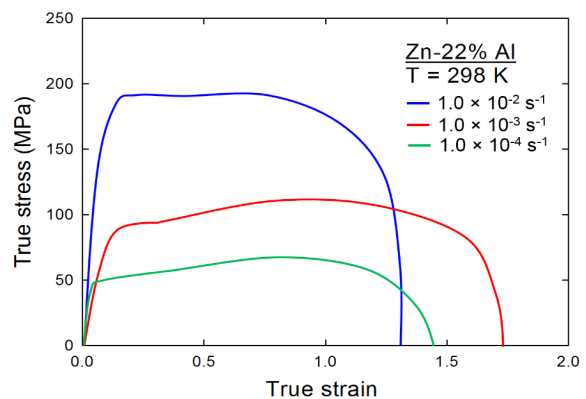


**Fig. 3.** True stress-true strain curves for the Zn-22% Al alloy tested at room temperature.

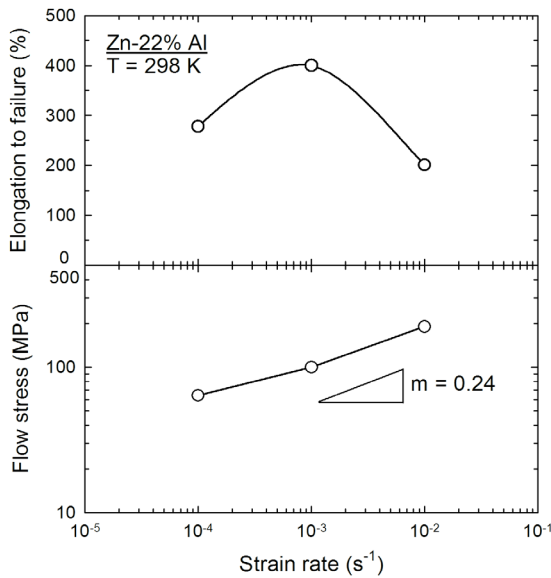


**Fig. 4.** Elongations to failure (upper) and flow stress (lower) versus strain rate for the Zn-Al alloy tested at room temperature.

[22—27,29—31]. Moreover, a reasonably consistent value of  $m \approx 0.35$  was measured through nanoindentation testing in an ultrafine-grained Zn-22% Al alloy after HPT [40].

The stress-strain curves in Fig. 3 show that there is a strain rate dependency of yield strength where the flow stress is higher at faster strain rate during testing. It is also apparent that the Zn-Al alloy demonstrates reasonably stable plateau stresses so that excellent ductility is achieved during deformation at room temperature.

The alloy exhibited elongations of  $>200\%$  at all strain rates as shown in an upper plot of Fig. 4 and a maximum elongation of  $400\%$  was observed at  $10^{-3} \text{ s}^{-1}$  in the present experiments. The result suggests the ultrafine-grained Zn-22% Al alloy demonstrates true room-temperature superplasticity and the significant superplastic elongation is the highest recorded in Zn-22% Al alloy at room temperature to date. From the lower curve in Fig. 4, the strain rate sensitivity,  $m$ , of  $\sim 0.24$  was calculated under the experimental conditions. Although this value is lower than  $m \approx 0.5$  measured in the alloy showing excellent superplasticity at  $473 \text{ K}$  [8], it is in good agreement with the earlier reports demonstrating  $m \approx 0.2\text{--}0.4$  for superplastic-type characteristics in Zn-22% Al alloys when testing in tension at room temperature [22—27,29—31]. Moreover, a reasonably consistent value of  $m \approx 0.35$  was measured through nanoindentation testing in an ultrafine-grained Zn-22% Al alloy after HPT [40].

#### 4. Discussion

The present study demonstrated the feasibility of producing an ultrafine-grained Zn-22% Al alloy by means of conventional heat treatment and subsequent cold rolling. The alloy was tested in tension at room temperature and exhibited a room-temperature superplastic elongation of  $400\%$  at a strain rate of  $10^{-3} \text{ s}^{-1}$ . This finding is attributed to the nature of a Zn-22% Al eutectoid alloy having low melting temperature leading to fast diffusion activity at room temperature.

In practice, the alloy was tested at  $298 \text{ K}$  which is reasonably high homologous temperature of the order of  $\sim 0.43T_m$  so that GBS accommodated by the motion of intragranular dislocations controlled by grain boundary diffusion is a viable deformation process at room temperature. It is supported by an early report showing GBS occurs in superplastic flow at lower temperatures when the grain sizes are reduced in a number of metallic, intermetallic and ceramic systems [41]. Moreover, there are reports showing direct evidence for the occurrence of GBS within the room-temperature superplastic regime by using an atomic force microscope (AFM) [42,43] and using SEM [22].

There are numbers of experiments reporting reasonably high  $m$  values of over  $0.2$  during room-temperature deformation in a series of Zn-Al alloys with different Al content [34—38,44] (including Al-Zn alloys [45,46]) and it is worth summarizing the data with the values of  $m$  in Table 1 where a processing route, grain size, testing method for measuring  $m$ , strain rate range and maximum elongation are listed in each material. It is apparent that all alloys recording high  $m$  values in a range of  $0.22\text{--}0.4$  at room temperature when containing grain sizes in the submicrometer range and most alloys demonstrated high elongations such as at least  $100\%$  so that most reports concluded there is an occurrence of room-temperature superplasticity in the alloys. However, most of the reported elongations are not as high as generally recognized elongations in superplasticity of  $\sim 400\%$  and it may be appropriate to describe as superplastic-like ductility whereas it is important to state that the measured elongations of samples are depending in part on the dimensions of the specimen gauge [47]. Nevertheless, the present investigation showed an elongation to failure of  $400\%$ , thereby concluding the exhibition of true superplasticity at room temperature in the Zn-22% Al alloy after conventional heat treatment followed by cold-rolling.

On the other hand, the  $m$  value lower than  $0.5$  for a theoretical superplastic model may be attributed to the existence of a threshold stress,  $\sigma_{th}$ , which was reported earlier in a Zn-22% Al alloy after ECAP and tested at room temperature [24,48]. In practice, an effective stress for plastic deformation is expressed as,  $\sigma - \sigma_{th}$ , where  $\sigma$  is the applied stress. Then, superplastic flow is represented by a relationship in which the steady-state strain rate,  $\dot{\epsilon}$ , is expressed as [49]

$$\dot{\epsilon} = \frac{AD_{gb}Gb}{kT} \left(\frac{b}{d}\right)^2 \left(\frac{\sigma - \sigma_{th}}{G}\right)^2 \quad (1)$$

where  $A$  is a dimensionless constant and was estimated as  $114$  for Zn-22% Al alloy [24],  $D_{gb}$  is the coefficient for grain boundary diffusion which is calculated with the activation energy for grain boundary diffusion in Zn of  $Q_{gb} = 60.5 \text{ kJ/mol}$  [50],  $G$  is the shear modulus,  $b$  is the Burgers vector,  $k$  is Boltzmann's constant and  $T$  is the absolute temperature. It should be recalled that there are two important parameters in the theoretical superplastic model as shown in eq. (1): the exponents of the inverse grain size,  $p$ , of  $2$  and the stress,  $n = (\partial \ln \dot{\epsilon} / \partial \ln \sigma = 1/m)$ , of  $2$  [49]. Thus, in the theoretical model, there is a linear relationship between  $\sigma$  and  $\dot{\epsilon}^{1/2}$  and the value of  $\sigma_{th}$  appears as an intercept at  $\dot{\epsilon} = 0$  of the trend line in a plot of  $\sigma$  vs.  $\dot{\epsilon}^{1/2}$ . Figure 5 displays a plot

**Table 1.** A list of Zn-Al alloys after different processing showing high values of strain sensitivity, *m*, at specific strain rate ranges and maximum elongations at room temperature measured in different testing methods

Material (wt.%)	Processing	Grain size (μm)	Testing method	<i>m</i>	Strain rate range (s <sup>-1</sup> )	Maximum elongation (%)	References
Al-30Zn	HPT for 5 turns at RT	~0.38	Tensile testing	~0.29	10 <sup>-4</sup> - 10 <sup>-3</sup>	~160%	Valiev <i>et al.</i> [45]
Al-30Zn	HPT for 5 turns at RT	~0.38	Microindentaion testing	~0.22	6.25 × 10 <sup>-5</sup> -1.75 × 10 <sup>-2</sup>	-	Chinh <i>et al.</i> [46]
Zn-0.3Al	Cold rolling	1	-Tensile testing until strain of 10% -Tensile testing until strain of 2.5%	0.41 0.32	10 <sup>-4</sup> - 10 <sup>-3</sup> 10 <sup>-6</sup> - 10 <sup>-4</sup>	1400	Ha <i>et al.</i> [34,35]
Zn-0.4Al	Cold rolling	~0.6	Tensile testing	0.4-0.5	10 <sup>-4</sup> - 10 <sup>-3</sup>	~500	Naziri and Pearce [36]
Zn-2Al Zn-10Al Zn-22Al Zn-50Al	Casting + quenching + annealing at 523K	~1	Tensile testing	0.4 0.43 0.45 0.43	10 <sup>-3</sup> - 10 <sup>-2</sup>	400 1250 1300 900	Kaibyshev <i>et al.</i> [37]
Zn-5Al	ECAP for 8p at RT	0.11-0.54	Tensile testing	0.25	10 <sup>-4</sup> - 10 <sup>-2</sup>	520	Demirtas <i>et al.</i> [44]
Zn-20Al	Hot rolling + quenching	0.55	Tensile deformation at <i>in-situ</i> TEM	0.25	10 <sup>-3</sup> -10 <sup>-1</sup>	-	Naziri <i>et al.</i> [38]
Zn-22Al-2Cu	Cold rolling at 293K	~0.3	Tensile testing	0.3	10 <sup>-4</sup> - 10 <sup>-3</sup>	~135	Torres-Villaseñor and Negrete [39]
Zn-22Al	TMCP (Rolling)	1.3	Tensile testing	0.3	10 <sup>-5</sup> - 10 <sup>-4</sup>	200	Tanaka <i>et al.</i> [22]
Zn-22Al	TMCP (Extrusion)	~0.9	Tensile testing	0.3	10 <sup>-5</sup> - 10 <sup>-2</sup>	~190	Tanaka <i>et al.</i> [23]
Zn-22Al	TMCP (Extrusion) + Cold rolling at RT	1.25	Tensile testing	0.25	10 <sup>-5</sup> - 10 <sup>-2</sup>	~300	Tanaka and Higashi [25]
Zn-22Al	-TMCP (Extrusion) -TMCP (Rolling)	1.84 1.16	Tensile testing	~0.33	10 <sup>-4</sup> - 10 <sup>-3</sup> 10 <sup>-4</sup> - 10 <sup>-2</sup>	~210 ~170	Tanaka and Higashi [27]
Zn-22Al	FSP	0.6	Tensile testing	0.25	10 <sup>-4</sup> - 10 <sup>-2</sup>	150	Hirata <i>et al.</i> [29]
Zn-22Al	ECAP for 4p at RT	0.35	Tensile testing	0.25	10 <sup>-4</sup> - 10 <sup>-2</sup>	~240	Tanaka and Higashi [24], Tanaka <i>et al.</i> [26]
Zn-22Al	-Quenching + aging at RT -ECAP for 8p at RT -Cryo-rolling at 203K	0.35 0.55 0.25	Tensile testing	0.38 0.35 0.32	10 <sup>-2</sup> - 10 <sup>-1</sup> 10 <sup>-2</sup> - 10 <sup>-1</sup> 10 <sup>-3</sup> - 10 <sup>-2</sup>	125 335 315	Xia <i>et al.</i> [30]
Zn-22Al	ECAP for 4p at 623K + 4p at RT	0.15-0.21	Tensile testing	0.3	3 × 10 <sup>-2</sup> - 2 × 10 <sup>-1</sup>	400	Demirtas <i>et al.</i> [31]
Zn-22Al	HPT for 5 turns at RT	0.35	Nanoindentation	0.226– 0.256	10 <sup>-4</sup> - 10 <sup>-3</sup>	-	Choi <i>et al.</i> [40]
Zn-22Al	Solutionizing + cold rolling	~0.63	Tensile testing	0.24	10 <sup>-3</sup>	400	This study

of  $\sigma$  vs.  $\epsilon^{1/2}$  for the Zn-22% Al alloy constructed using the testing data shown in Figs. 3 and 4 and the threshold stress of  $\sigma_{th}=52.5$  MPa is estimated under the present testing conditions. This value is in agreement with the reported value of 46 MPa for a Zn-22% Al alloy tested at 303 K and it is much higher than 2 MPa for the same alloy when testing at 473 K [48]. Therefore, the analysis suggests the theoretical superplastic model with  $m=0.5$  developed for high temperature superplasticity is applicable for room-temperature superplastic flow of Zn-22% Al alloy when taking into account of the threshold stress which tends to appear intensely in superplastic flow at ambient temperature.

Finally, it is worthwhile to mention that, although the influence may not be as critical as the threshold stress, the lower value of  $m$  is also caused in part by the level of GBS attributed to the microstructural homogeneity of Al- and Zn-rich phases in the sample. Early GBS measurement by TEM showed there is different levels of contributions of sliding to the entire plastic strain at individual interfaces during high temperature deformation and a maximum contribution was observed on the Zn-Zn interfaces and slightly less on the Zn-Al interfaces while the Al-Al interfaces exhibited a minimum contribution of GBS in a conventional Zn-22% Al alloy [51] and after ECAP [17,18,20]. In a very recent report, room-temperature plastic deformation by nanoindentation examinations revealed the homogeneity in distributions of the Zn and Al phases is strongly correlated with the change in the  $m$  value [40]. In practice, the agglomerations of Zn- and Al- phases in a Zn-22% Al alloy in an early stage of HPT leads to high  $m$  value than the microstructure involving the homogeneously distributed two phases after additional HPT processing. Accordingly, the present study synthesized an ultrafine-grained microstructure with homogeneous distributions of Zn- and Al- phases as shown in Fig. 2 which may lead to reduction in the level of overall GBS to the total strain, thereby lowering the  $m$  value in true superplasticity at room temperature.

## 5. Summary and conclusions

The present study demonstrated the synthesis of an ultrafine-grained Zn-22% Al eutectoid alloy through the solution treatment and conventional thermo-mechanical processing. The microstructure consists of homogeneously distributed Zn and Al grains with average sizes of  $\sim 0.63$   $\mu\text{m}$ . The alloy demonstrated true room-temperature superplasticity with the highest elongation to failure of 400% at  $10^{-3}$   $\text{s}^{-1}$  and a strain rate sensitivity of  $m \approx 0.24$ . The detailed analysis concluded the theoretical superplasticity model is applicable to explain room-temperature superplastic flow in the Zn-22% Al alloy by estimation of the threshold stress for the alloy during deformation and the consideration of grain boundary sliding contribution to the total strain which is attributed to the homogeneous distribution of Zn and Al phases in the material.

*Acknowledgements.* This work was supported in part by Takenaka Corp. and in part by the NRF Korea funded by MoE under Grant No. NRF-2014RIA1A2057697 (MK).

## References

1. T.G. Langdon, J. Mater. Sci. **44**, 5998 (2009).
2. T.G. Langdon, Mater. Sci. Eng. **A174**, 225 (1994).
3. H. Ishikawa, D.G. Bhat, F.A. Mohamed, T.G. Langdon, Metall. Trans. **8A**, 523 (1977).
4. M.M.I. Ahmed, T.G. Langdon, Metall. Trans. **8A**, 1832 (1977).
5. K. Higashi, T. Ohnishi, Y. Nakatani, Scripta Metall. **19**, 821 (1985).
6. Y. Ma, T.G. Langdon, Metall. Mater. Trans. A **25A**, 2309 (1994).
7. F.A. Mohamed, T.G. Langdon, Acta Metall. **23**, 117 (1975).
8. H. Ishikawa, F.A. Mohamed, T.G. Langdon, Phil. Mag. **32**, 1269 (1975).
9. F.A. Mohamed, M.M.I. Ahmed, T.G. Langdon, Metall. Trans. **8A**, 933 (1977).
10. M.A. Meyers, A. Mishra, D.J. Benson, Prog. Mater. Sci. **51**, 427 (2006).
11. ROC Patent Publication No. I273023.
12. R.Z. Valiev, T.G. Langdon, Prog. Mater. Sci. **51**, 881 (2006).
13. R.S. Mishra, M.W. Mahoney, S.X. McFadden, N.A. Mara, A.K. Mukherjee, Scripta Mater. **42**, 163 (2000).
14. A.P. Zhilyaev, T.G. Langdon, Prog. Mater. Sci. **53**, 893 (2008).
15. K. Makii, Y. Mimura, H. Ueda, Japan Patent Office (1999) 11-222643.
16. P. Kumar, C. Xu, T.G. Langdon, Mater. Sci. Eng. **A410-411**, 447 (2005).
17. M. Kawasaki, T.G. Langdon, Mater. Trans. **49**, 84 (2008).
18. M. Kawasaki, T.G. Langdon, Mater. Sci. Eng. **A503**, 4851 (2009).
19. M. Kawasaki, T.G. Langdon, Mater. Sci. Eng. **A528**, 6140 (2011).
20. M. Kawasaki, T.G. Langdon, Mater. Trans. **53**, 87 (2012).
21. M.R. Azpeitia, E.E.M. Flores, G. Torres-Villaseñor, J. Mater. Sci. **47**, 6206 (2012).
22. T. Tanaka, K. Makii, A. Kushibe, K. Higashi, Mater. Trans. **43**, 2449 (2002).
23. T. Tanaka, K. Makii, A. Kushibe, M. Kohzu, K. Higashi, Scripta Mater. **49**, 361 (2003).
24. T. Tanaka, K. Higashi, Mater. Trans. **45**, 1261 (2004).
25. T. Tanaka, K. Higashi, Mater. Trans. **45**, 2547 (2004).
26. T. Tanaka, H. Watanabe, M. Kohzu, K. Higashi, Mater. Sci. Forum **447-448**, 489 (2004).
27. T. Tanaka, M. Kohzu, Y. Takigawa, K. Higashi, Scripta Mater. **52**, 231 (2005).
28. P. Kumar, C. Xu, T.G. Langdon, Mater. Sci. Eng. **A429**, 324 (2006).
29. T. Hirata, T. Tanaka, S.W. Chung, Y. Takigawa, K. Higashi, Scripta Mater. **56**, 477 (2007).
30. S.H. Xia, J. Wang, J.T. Wang, J.Q. Liu, Mater. Sci. Eng. **A493**, 111 (2008).
31. M. Demirtas, G. Purcek, H. Yanar, Z.J. Zhang, Z.F. Zhang, Mater. Sci. Eng. **A620**, 233 (2014).
32. K. Makii, S. Furuta, K. Aoki, A. Kushibe, T. Tanaka, K. Higashi, Mater. Sci. Forum **447-448**, 497 (2004).
33. A. Kushibe, Y. Takigawa, K. Higashi, K. Aoki, K. Makii, T. Takagi, Mater. Sci. Forum **551-552**, 583 (2007).

34. T.K. Ha, W.B. Lee, C.G. Park, Y.W. Chang, *Metall. Mater. Trans. A* **28A**, 1771 (1997).
35. T.K. Ha, J.R. Son, W.B. Lee, C.G. Park, Y.W. Chang, *Mater. Sci. Eng.* **A307**, 98 (2001).
36. H. Naziri, R. Pearce, *Acta Metall.* **22**, 1321 (1974).
37. O.A. Kaibyshev, B.V. Rodionov, R.Z. Valiev, *Acta Metall.* **26**, 1877 (1978).
38. H. Naziri, R. Pearce, M.H. Brown, K.F. Hale, *Acta Metall.* **23**, 489 (1975).
39. G. Torres-Villaseñor, J. Negrete, *Mater. Sci. Forum* **243–245**, 553 (1997).
40. I.-C. Choi, Y.-J. Kim, B. Ahn, M. Kawasaki, T.G. Langdon, J.-I. Jang, *Scripta Mater.* **75**, 102 (2014).
41. S.X. McFadden, R.S. Mishra, R.Z. Valiev, A.P. Zhilyaev, A.K. Mukherjee, *Nature* **398**, 684 (1999).
42. Y. Huang, T.G. Langdon, *J. Mater. Sci.* **37**, 4993 (2002).
43. Y. Huang, T.G. Langdon, *Mater. Sci. Eng.* **A358**, 114 (2003).
44. M. Demirtas, G. Purcek, H. Yanar, Z.J. Zhang, Z.F. Zhang, *J. Alloys Compds* **623**, 213 (2015).
45. R.Z. Valiev, M.Yu. Murashkin, A. Kilmametov, B. Straumal, N.Q. Chinh, T.G. Langdon, *J. Mater. Sci.* **45**, 4718 (2010).
46. N.Q. Chinh, T. Csanádi, T. Gyóri, R.Z. Valiev, B.B. Straumal, M. Kawasaki, T.G. Langdon, *Mater. Sci. Eng.* **A543**, 117 (2012).
47. Y.H. Zhao, Y.Z. Guo, Q. Wei, T.D. Topping, A.M. Dangelewicz, Y.T. Zhu, T.G. Langdon, E.J. Lavernia, *Mater. Sci. Eng.* **A525**, 68 (2009).
48. T. Tanaka, Y. Takigawa, K. Higashi, *Scripta Mater.* **58**, 643 (2008).
49. T.G. Langdon, *Acta Metall. Mater.* **42**, 2437 (1994).
50. H.J. Frost, M.F. Ashby, *Deformation-Mechanism Maps*, (Pergamon Press Oxford, 1982) p. 44.
51. P. Shariat, R.B. Vastava, T.G. Langdon, *Acta Metall.* **30**, 285 (1982).